SLAC Proposal No. 11
May 1966

PROPOSAL TO STUDY ρ^0 PHOTOPRODUCTION FROM COMPLEX NUCLEI AT FORWARD ANGLES

A. Boyarski, F. Bulos, R. Diebold, R. Larsen
D. Leith and B. Richter
Stanford Linear Accelerator Center, Stanford, California

L. Kaufman, V. Perez-Mendez and A. Stetz
Lawrence Radiation Laboratory, Berkeley, California

SUMMARY

A wire spark chamber spectrometer system is proposed to study the forward production of ρ^0's from several different complex nuclei by 8 GeV photons. The production of other particles, e.g., $\phi(1020) \rightarrow K^+ K^-$ and $f(1250) \rightarrow \pi^+ \pi^-$ from carbon will also be studied, as will be the energy dependence of the ρ^0 photoproduction cross section. The photoproduction target will be placed in the monochromatic photon beam of End Station B. The beam remaining after the target will be absorbed by a tungsten stopper placed in the gap of one of the SLAC 18D72 bending magnets, which together with wire chambers located behind the magnet will measure the angle and momentum of the decay pions. Magnetostrictive readout of the wire chambers will be used and the digitized information will be placed directly onto magnetic tape. Preliminary results will be obtainable during the runs and final results within a few months. We estimate that 270 hours of machine time are required for this study, 220 hours at 180 bursts per second and 50 hours at a low rate for setup purposes. Operation of the monochromatic photon beam is needed for the experiment and, except for some of the setting up and an occasional background run, we shall need the positron beam. The equipment should be ready by December 1966.

I. MOTIVATION

The photoproduction of ρ^o mesons has been studied in the range $1 \lesssim k \lesssim 5$ GeV by a counter group[1] (hydrogen, carbon, aluminum and copper targets) and two hydrogen bubble chamber groups.[2,3] Several facets of the experimental data point to the process being dominated by the diffraction mechanism proposed by Berman and Drell[4] and indicated in Fig. 1:

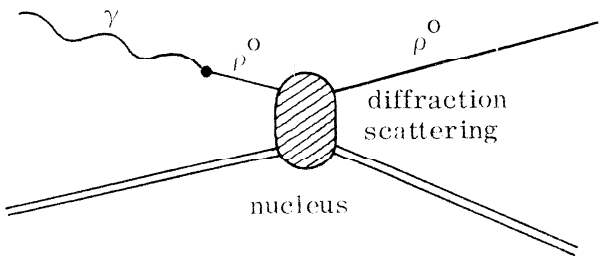

FIG. 1

(i) The total ρ cross section becomes constant at high energies.

(ii) The hydrogen differential cross section at 0^o goes roughly as

$$\left(\frac{d\sigma}{d\Omega}\right)_{0^o} \propto k^2$$

(iii) The variation of the hydrogen cross section as a function of t, the four-momentum transfer squared, is similar to that for πp elastic scattering.* (This point is related to the first two.)

(iv) The variation of $d\sigma/d\Omega$ extraplated to $t = 0$ as a function of the atomic number A is similar to that for elastic p-nucleus scattering,[5] namely $A^{1.6}$.

At high energies the ρ cross section represents a sizable fraction of the total cross section for the photoproduction of strongly interacting particles; at 4.2 GeV

---

*The unadorned one pion exchange photoproduction differential cross section does not fit the data well. A large final state absorption à la Gottfried-Jackson can be invoked to modify the OPE cross section to reproduce the q^2 distribution rather well (see Fig. 6 of the CEA preprint, Ref. 2). If, however, one were to assume the process to be OPE + absorption, the value obtained by Ref. 2 for $\Gamma_{\gamma\pi\rho}$ would be 10 MeV for $k > 3.5$ GeV; this is 14 times larger than the (95% confidence) upper limit given by Huson et al. [Phys. Letters 20, 91 (1966)] and 100 times larger than the SU_6 prediction.

the CEA bubble chamber group gets 22 μbarns for ρ production out of about 70 μbarns total.

The experiment described in this proposal extends the CEA counter experiment in several ways:

(i) Higher energy

(ii) Larger range of A: Li^7, C^{12}, Al^{27}, Cu^{64}, Ag^{108}, and Pb^{207}

(iii) Complex nuclei cross sections as a function of t (instead of just the 0^o cross sections)

(iv) Better resolution in photon energy, ρ mass, etc.

Such an experiment would allow one to study the ρ-nucleus cross section in a manner similar to that of Bellettini et al.,[5] who studied the 20 GeV/c proton-nucleus differential cross sections at small values of t. They used eight different nuclei as targets, measuring 10,000 to 40,000 elastic scattering events for each target. They observed a rapid fall-off with t at very small angles characteristic of Coulomb and coherent diffraction scattering; using the optical model formula

$$\frac{d\sigma}{dt} \propto e^{-R^2 t/4}$$

they obtained for the lighter elements values of the nuclear radius R similar to those given by Hofstadter. If the proton-nucleus small angle fall-off is characterized by e^{-q^2/q_o^2}, then the data for $12 \leq A \leq 207$ can be fit with

$$q_o = 260/A^{0.3} \text{ MeV/c.}$$

This has been evaluated for several elements and, together with the corresponding angle for our energy of 8 GeV, is shown in Table 1.

TABLE 1

Element	A	$q_o = 260/A^{0.3}$	θ_o (8 GeV)
Beryllium	9	135 MeV/c	0.96^o
Carbon	12	123	0.88^o
Aluminum	27	97	0.70^o
Copper	63.5	75	0.54^o
Silver	107.9	64	0.46^o
Lead	207.2	52	0.37^o

At larger angles Bellettini et al. observe a much less steep dependence with a slope characteristic of free nucleon-nucleon scattering, presumably from incoherent elastic scattering off the individual nucleons. Fitting the large angle data to curves of the form e^{-10t} and comparing with the free nucleon-nucleon cross section gave an effective number of free nucleons N(A) acting as scattering centers. The fraction N(A)/A represents the probability that a high energy proton crosses the nucleus without being absorbed by inelastic interactions; in the optical model this is just the transparency of the nucleus and is given by $1 - (\sigma_{abs}/\pi R^2)$, where σ_{abs} is the total inelastic proton-nucleus cross section. The values of σ_{abs} obtained in this indirect way agree very closely with the directly observed experimental values.

Drell and Trefil[6] use the total cross sections for proton-nucleus scattering as a function of A to calculate a total nucleon-nucleon cross section of 45 ± 5 mbarns in good agreement with the observed number. They then use the CEA counter data[1] on ρ^o photoproduction at 0^o to calculate the total ρ^o-nucleon cross section as 80 ± 14 mbarns. The accuracy of this calculation would be greatly increased by an accurate (5 or 10%) measurement of ρ^o photoproduction from lead.

Unitary symmetry predicts that photoproduction of vector mesons via the diffraction mechanism should be in the ratio 9:2:1 for ρ^o, ϕ and ω. The $\rho^o:\omega$ cross section ratios obtained by the hydrogen bubble chambers are compatible with this prediction, e.g., the CEA group[2] gives 6.7 ± 1.1 for $2.5 < k < 6$ GeV (important contributions to ω production in hydrogen are also expected from one pion exchange). The ratio of $\rho^o:\phi$ photoproduction is difficult to estimate from the available bubble chamber results, but it appears the ϕ production is $\lesssim 1\,\mu b$, i.e., down by a factor of 4 or more from the unitarity symmetry prediction. The experimental values of the $\rho^o:\phi:\omega$ ratios make an interesting test of the assumptions which went into the theoretical calculations, namely, that the electromagnetic current is pure octet and that the vector meson nonet is discussed correctly as a mixed SU_3 octet and singlet. Because of the great interest in the $\rho^o:\phi$ production ratio, we plan to make a special small angle run looking for ϕ's.*

Higher mass mesons may also be photoproduced from complex nuclei and we plan to make special runs sensitive to particles with $M \lesssim 1.6$ GeV which decay

* If backgrounds allow, we may be able to crudely measure ω^o production by looking at the π^+ and π^- from ω decay; these pions have a broad effective-mass peak in the region 350 to 500 MeV.

via $\pi^+ \pi^-$. This decay mode resticts* us to states having $J^P = 1^-, 2^+, 3^-$, etc. (not 0^+ since $J_z = \pm 1$ for particles photoproduced coherently in the forward direction). We may photoproduce not only vector mesons via a diffraction mechanism, but also 2^+ objects such as the $f^o(1250)$ [a similar change in spin may have been observed[7] in the diffraction-like production of $A_1(1080)$ enhancement by pions incident on complex nuclei $(0^- \rightarrow 1^+)$]. The DESY bubble chamber group recently reported[8] a cross section of $\sim 1\,\mu$barn for $\gamma p \rightarrow f^o p$ averaged over $2 \leq k \leq 5.5$ GeV.

In summary, the experiment should allow the following:**

(i) Verification of diffraction as the dominant mechanism from the variation of cross section with energy, momentum transfer, and atomic number.

(ii) Determination of effective nuclear radii for coherent photoproduction.

(iii) Absorptive cross section for ρ^o's incident on nuclei.

(iv) Better Drell-Trefil determination of the total ρ^o-nucleon cross section due to the use of a wider range of A as target.

(v) Better extrapolation of various cross sections to the high energy limit where they can be compared with various theoretical predictions, e.g., the SU_{6_W} prediction $\sigma_{\rho N} = \sigma_{\pi N}$.

(vi) Comparison of ρ^o and ϕ photoproduction; and

(vii) Measurement of the photoproduction cross sections for higher mass states having $J^P = 1^-, 2^+, 3^-$, etc.

---

*The restriction due to the decay mode represents no great loss since the matrix element for non-spin flip (necessary for coherence) photoproduction of particles with $J^P = 1^+, 2^-, 3^+$, etc. (different intrinsic parity than the photon with $J^P = 1^-$) goes to zero in the forward direction and the cross section is suppressed by a factor θ^2. The photoproduction of $1^-, 2^+, 3^-$, etc. particles is not suppressed in this manner, the spin angular momentum being picked up from the orbital angular momentum.

**Note added in proof. We have just received a preprint from Marc Ross and Leo Stodolsky (BNL 10146) which discusses in detail many of the points mentioned above. Using a diffraction dissociation model together with the existing ρ-photoproduction data they obtain ρ-nucleon cross sections and the effective ρ-photon coupling; the implications of the small ϕ cross section are also discussed. They suggest several experiments, many of which are covered by this proposal.

II. EXPERIMENTAL METHOD

The experimental arrangement is shown in Fig. 2. The monochromatic photon beam,[9] produced by the annihilation of positrons in a 30 cm liquid hydrogen target, is collimated to 1 cm wide by 10 cm high at the photoproduction target, ~ 25 meters downstream from the annihilation target. The multiple scattering of electrons in the hydrogen target before annihilation gives an uncertainty in the photon energy of about ± 2%; the 1 cm width of the beam at 25 meters also represents a ± 2% uncertainty, giving a total σ_k/k of ~ 3%. The positrons also bremsstrahlung in the hydrogen target giving a background to the monochromatic peak. Most of our running will be with 8 GeV monochromatic photons produced by positrons of the maximum easily obtainable energy, say 11 or 12 GeV. According to Chadwick[10] this would give approximately as many bremsstrahlung photons above 1 GeV as monochromatic photons, namely, ~ 500/pulse.

The unused photon beam is stopped by a tungsten plug located at the entrance to the bending magnet. The plug has a rectangular cross section, filling the magnet aperture in the vertical direction, and having a width determined primarily by the soft photon background. As discussed in Appendix C, a stopper width of 12 cm (± 6 cm = ± 18 radiation lengths) should be more than adequate to reduce this background to an acceptable level.

The two ρ-decay pions are momentum analyzed by one of the standard SLAC bending magnets in conjunction with wire chambers. These magnets are a Brookhaven type 18D72, having a 15 cm × 45 cm aperture, a length of 1.83 meters, and a maximum field of ~ 20 kG. The field and target-stopper distance are determined by the effective $\pi\pi$ mass interval desired; typical values when studying the ρ region are 20 kG and 1.2 meters.

As shown in Fig. 2, three pairs of trigger counters will be placed behind the magnet. We will require the firing of at least four or five of the six counters as a signature (the two π's may cross near the counter pairs and then pass through only one of the two counters). Four sets of wire chambers will be placed behind the magnet, each set consisting of four planes rotated at 45° with respect to one another; such a system is highly redundant, allowing resolution of ambiguities as well as numerous checks on the data. The momentum is determined by the wire chamber measurement of the particle position and direction after bending in the magnetic field, together with the horizontal target position. No counters

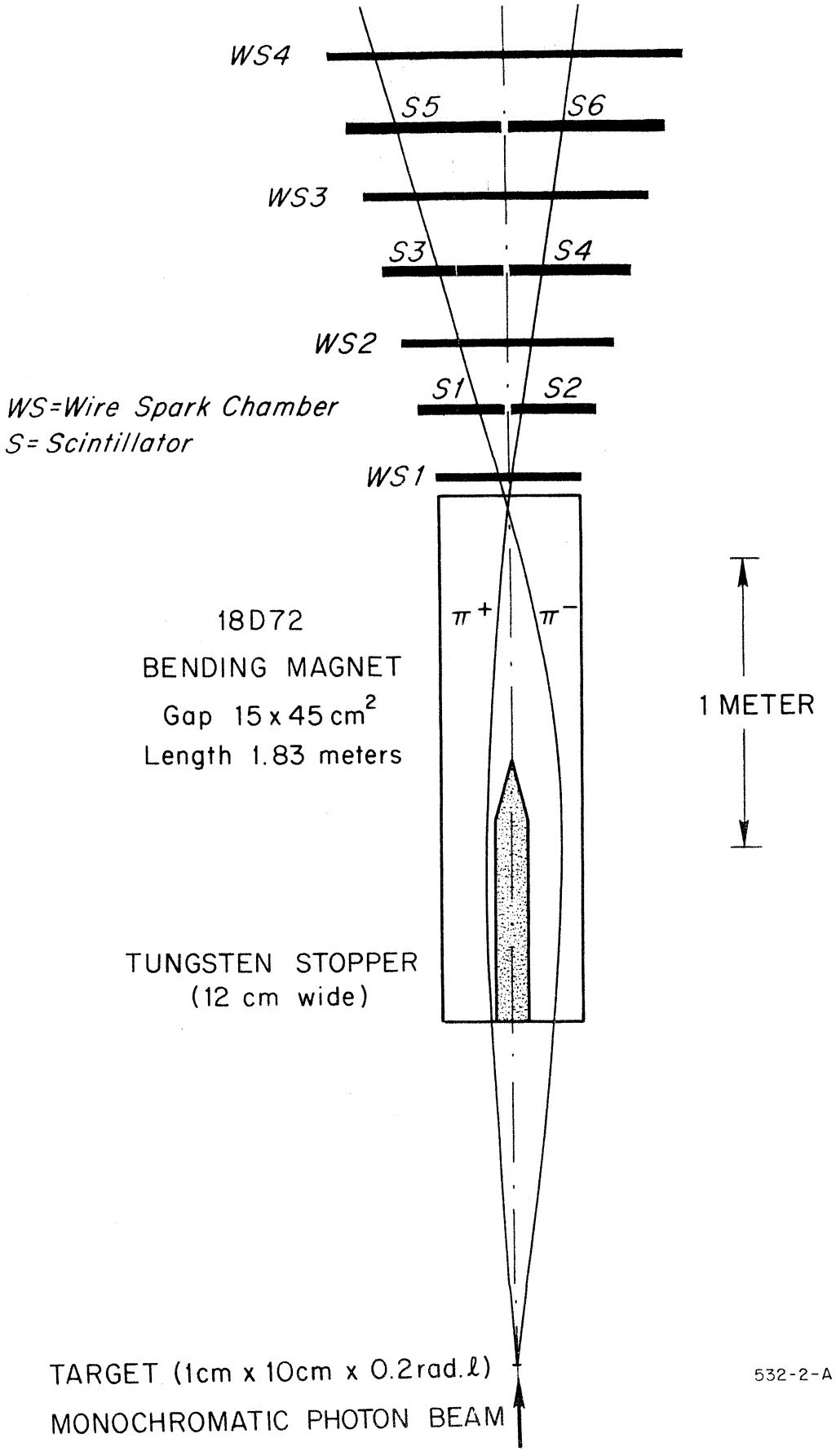
WS4
S5
S6
WS3
S3
S4
WS2
S1
S2
WS1
WS=Wire Spark Chamber
S=Scintillator
18D72
BENDING MAGNET
Gap 15 x 45 cm²
Length 1.83 meters
π+
π−
1 METER
TUNGSTEN STOPPER
(12 cm wide)
TARGET (1cm x 10cm x 0.2rad.ℓ)
MONOCHROMATIC PHOTON BEAM
532-2-A

Fig. 2

or wire chambers can be placed in front of the magnet because of the large amount of background (low energy electrons from the target).

Wire chambers were chosen for the measurements since counter hodoscopes are impractical because of the fine spatial resolution required over a large area. Sonic chambers have difficulty with multiple tracks, and it would not be easy to split the chambers in two, one for each π, since the two tracks are crossing each other in the measuring region. The events are not so complicated as to warrant visual spark chamber techniques. Wire chambers with magnetostrictive readout[11] are capable of recording multiple-spark events with a two-spark resolution of $\lesssim$ 3 mm. By adjusting the operating conditions properly a particle can be made to fire two or three wires giving the position to $\pm$ 1/3 of the wire spacing of $\sim$ 1 mm. Up to four sparks per plane (allowing up to two spurious sparks) will be recorded on magnetic tape through the use of specialized electronics. The chambers and recording electronics are described in more detail in Appendix D. The electronics may be capable of some display of the events allowing on-line checking of the data; in any case, we anticipate taking the magnetic tape directly to a large computer for preliminary analysis during the runs.

No special counters are planned to discriminate between various types of particles. The geometric and kinematic fitting will eliminate the vast majority of background particles. Background runs will also be made. The narrow width of the ϕ (Γ = 3 MeV; our experimental resolution has approximately the same width) should enable its detection even with $\pi\pi$ (effective mass $\sim$ 360 MeV) background present.

The first order optics of the magnet system is discussed in Appendix A. For ρ's decaying near $\theta' = 90^{\circ}$ (center-of-mass angle), the decay pions cross each other on the axis (defined by the ρ direction) at a distance beyond the magnet which depends only upon the effective $\pi\pi$ mass (independent of small changes in θ' and k). For m_{ρ} = 750 MeV and a center-of-mass decay angle differing from 90° by 30° (corresponding roughly to the acceptance of the system at the ρ mass), the crossing point is foreshortened to a point which corresponds to a 90° decay with $m_{\pi\pi} \approx 670$ MeV. Thus, if one has a large acceptance, only crude information on the effective mass can be obtained by simply using the crossing point coordinate.

Since the first order focusing is independent of photon energy (both the production and bending angles go as 1/k), the system is sensitive to π pairs produced by a wide range of photon energies.

The laboratory pion momentum is shown in Fig. 3 as a function of laboratory pion angle for several effective $\pi^+\pi^-$ masses with $E_{\pi^+} + E_{\pi^-} = 8$ GeV; tick marks are shown on the curves at 10^o center-of-mass decay angle intervals. Also shown is the 8 GeV $\phi(1020) \rightarrow K^+K^-$ curve.

The horizontal acceptance limits of the system are essentially defined by three considerations:

(i) The lead plug limits small angles.

(ii) The width of the magnet aperture limits the wide angles; this limit depends strongly on momentum, the low momentum particles being bent back before smashing into the magnet yoke.

(iii) The magnetic field sweeps particles with too low a momentum through a large angle, causing them to miss the trigger counters or smash into the magnet yoke; this limit depends somewhat upon the initial angle of the particle.

These limits have been plotted in Fig. 3 and used to calculate the acceptance discussed below. Eventually detailed computer calculations of the acceptance will need to be made in order to determine the optimum experimental conditions and, even more important, in order to interpret the experimental data.

For $m_\rho = 750$ MeV and 0^o production angle the apparatus is sensitive to $60^o \lesssim \theta' \lesssim 120^o$ which corresponds to 70% of the ρ decays ($\sin^2\theta'$ distribution for $J^P = 1^-$ aligned with $J_z = \pm 1$; for a 2^+ particle this becomes $\sin^2 2\theta$, 27% of which lies between 60^o and 120^o). This efficiency falls off on either side, being $\sim 30\%$ at $m_{\pi\pi} = 560$ and 940 MeV. The $m_{\pi\pi}$ acceptance can be shifted by adjusting the magnetic field and/or by moving the target back and forth. The acceptance of ρ's coming off at an angle in the horizontal direction falls to about 1/2 the forward value at $\theta_\rho \approx 2^o$ corresponding to $q_H \approx 280$ MeV/c. The vertical acceptance is limited by the pole faces at the magnet exit and severely limits the azimuthal angular range over which the ρ can decay and still have both pions pass through the magnet. The azimuthal acceptance for forward ρ's depends upon k and θ', typical acceptance being 6% for k = 8 GeV. This acceptance falls by a factor of ~ 2 for ρ's with a vertical component of momentum $q_V = 90$ MeV/c, a more severe limitation than that in the horizontal direction.

A considerable gain in mass and q^2 acceptance would be made if a magnet with larger aperture could be obtained, for example, one of the Berkeley Atlas

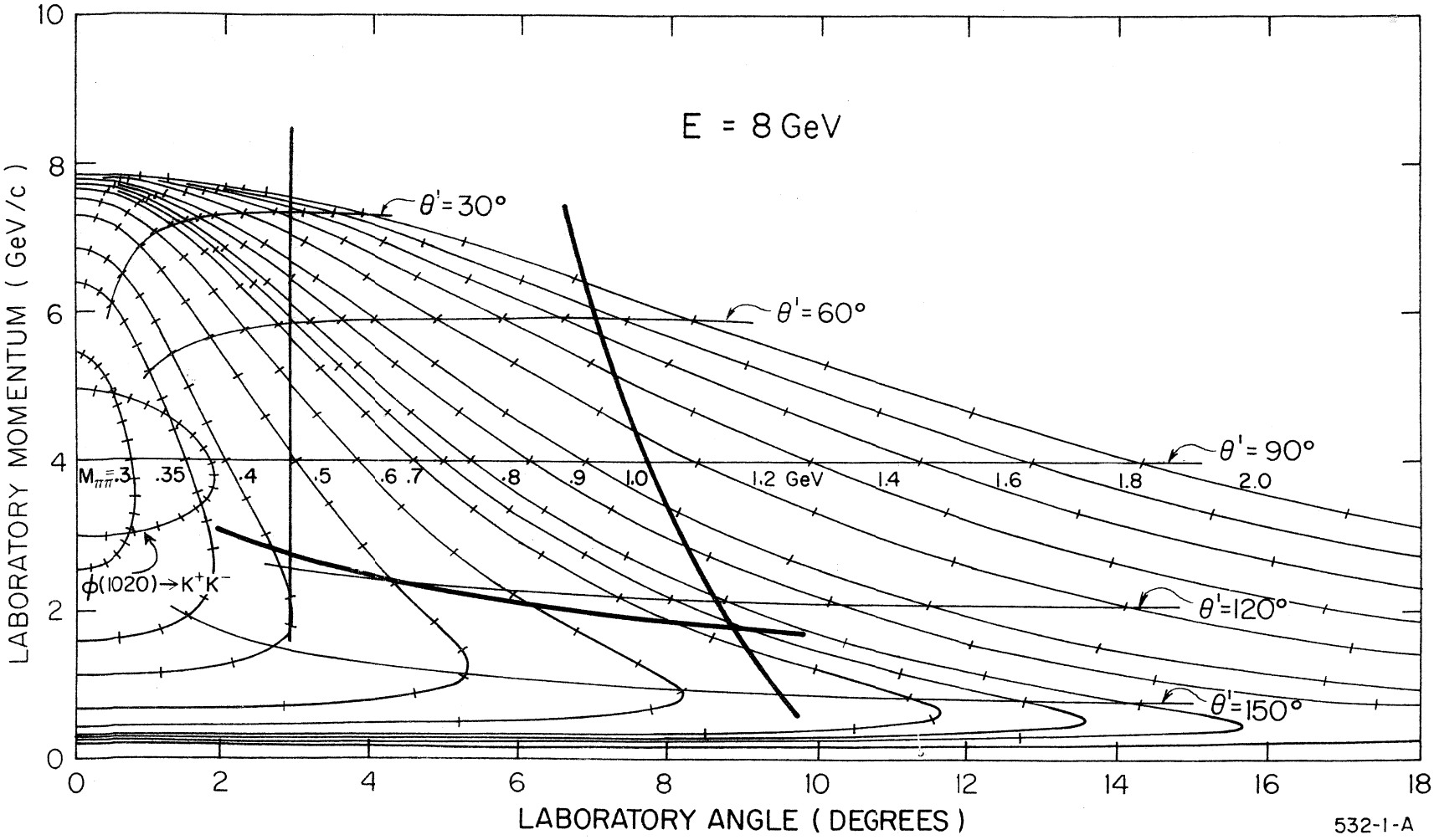
E = 8 GeV
θ'=30°
θ'=60°
θ'=90°
θ'=120°
θ'=150°
$M_{\pi\pi}$ .3 .35 .4 .5 .6 .7 .8 .9 1.0 1.2 GeV 1.4 1.6 1.8 2.0
φ(1020)→K⁺K⁻
LABORATORY MOMENTUM (GeV/c)
LABORATORY ANGLE (DEGREES)
0 2 4 6 8 10 12 14 16 18
0 2 4 6 8 10
532-1-A

Fig. 3

magnets or the SLAC 54-inch magnet with suitable pole pieces. The Atlas, with aperture 8 inches × 29 inches and a 36-inch length, could cover the mass range 500 to 1400 MeV in one run, and effective masses up to about 2 GeV could be studied. The vertical acceptance would nearly double as would the range of q_V.

The experimental resolution of the wire chamber-magnet system is discussed in detail in Appendix B, where it is assumed that the effective target full width is 1 cm (giving $\sigma = \pm 3$ mm) and the accuracy of the wire chamber measurements is $\sigma = \pm 0.5$ mm. Taking into account various correlations, the results at $k = 8$ GeV are typically

$$\sigma_k = \pm 1.5\%$$

$$\sigma_{m_\rho} = \pm 10 \text{ MeV}$$

$$\sigma_q = \pm 8 \text{ MeV/c}$$

Multiple scattering in the target (0.2 rad. lengths) gives additional uncertainties $\sigma_q = \pm 9$ MeV/c and $\sigma_{m_\rho} = \pm 7$ MeV.

The principal backgrounds are discussed in detail in Appendix C; it appears that none of them present serious difficulties:

1. Soft photons (mainly 0.5 to 3 MeV) escape laterally from the showers in the tungsten absorber. These photons then interact in the trigger counters giving random counts and sparks in the wire chambers. Monte Carlo calculations indicate that these photons can be reduced to an acceptable level by adjusting the stopper width.
2. Two or more strongly interacting particles photoproduced in the stopper will give false triggers. These particles are strongly attenuated by the tungsten and the false trigger rate should be quite reasonable. A rejection factor of about 50 from the geometric and kinematic fitting is expected for these false events and any remaining contamination can be determined by "empty target" runs.
3. Electrons and positrons pair produced in the photoproduction target occasionally come off at wide angles due to being pair produced at a very wide angle and/or singly scattered in the target. These particles miss the stopper and pass through the spectrometer system; they are the principal source of the singles counting rate. This background results in extraneous tracks for some of the events and an occasional random

coincidence yielding a background event consisting of two independent electrons (again the fitting should reject nearly all such events).

4. Neutrons do not appear to be troublesome.

The positron beam will be monitored to $\sim \frac{1}{2}\%$ by a toroidal current detector. Absolute calibration of the number of monochromatic photons will be obtained by taking out the tungsten stopper and using the apparatus to measure electron pairs.

III. COUNTING RATE

The number of ρ^{o}'s produced by monochromatic photons and detected by the apparatus can be expressed as :

$$N_\rho = N_\gamma N_T \sigma \eta ,$$

where N_γ is the number of monochromatic photons, N_T is the number of target particles/cm^2, σ is the total ρ photoproduction cross section, and η is the detection efficiency.

N_γ, the number of monochromatic photons

The number of monochromatic photons from positron annihilation is:

$$N_\gamma = N_{e^+} N_H \frac{d\sigma}{d\Omega} \Delta\Omega \eta_{LiH} .$$

For the number of positrons we take the somewhat conservative value

$$N_{e^+} = 10^{10} \text{ positrons/pulse.}$$

The thickness of the annihilation hydrogen target is limited by the allowable positron multiple scattering before annihilation:

$$\sigma_\theta \approx \frac{15 \text{ MeV}}{E_+} \sqrt{\frac{t}{2}} .$$

This uncertainty in angle leads to a broadening of the monochromatic peak:

$$\frac{\sigma_k}{k} = \sqrt{\frac{2k(E_+ - k)}{m_e E_+}} \sigma_\theta$$

$$= 0.089 \sqrt{t} \text{ for } E_+ = 11 \text{ GeV}, \; k = 8 \text{ GeV}.$$

Requiring a photon energy resolution of about $\pm 2\%$:

$$t = \left(\frac{1}{0.1}\,\frac{\sigma_k}{k}\right)^2$$

$$= 0.04 \text{ radiation length} = 2.3 \text{ gm/cm}^2 = 33 \text{ cm.}$$

This gives:

$$N_H = \frac{2.3}{1.008} \times 6.023 \times 10^{23} = 1.4 \times 10^{24}/\text{cm}^2 .$$

The annihilation cross section is given by[10] :

$$\frac{d\sigma}{d\Omega} = \frac{r_o^2}{2}\,\frac{\epsilon}{1-\epsilon}\left[\epsilon^2 + (1-\epsilon)^2\right]$$

$$= 3.98 \times 10^{-26}\,\frac{\epsilon}{1-\epsilon}\left[\epsilon^2 + (1-\epsilon)^2\right] \text{ cm}^2/\text{sterad},$$

where $\epsilon = k/E_+$ is the fraction of positron energy given to the photon. For $k = 8$ GeV, $E_+ = 11$ GeV, we have $\epsilon = 0.73$ giving:

$$\frac{d\sigma}{d\Omega} = 6.4 \times 10^{-26} \text{ cm}^2/\text{sterad.}$$

The solid angle for a target 1 cm wide by 10 cm high just outside End Station B ($\sim$ 90 ft = 27 meters from the annihilation target) is :

$$\Delta\Omega = \frac{1 \times 10}{(2700)^2} = 1.37 \times 10^{-6} \text{ sterad .}$$

The lithium hydride beam hardener will absorb some of the monochromatic photons. If one radiation length is used, the fraction of monochromatic photons which survive is :

$$\eta_{LiH} = e^{-7/9} = 0.46.$$

Thus, the number of monochromatic photons is :

$$N_\gamma \approx 10^{10} \times (1.4 \times 10^{24}) \times (6 \times 10^{-26}) \times (1.37 \times 10^{-6}) \times 0.46$$

$$= 530 \text{ monochromatic photons/pulse.}$$

N_T, the number of target particles/cm^2

The thickness of the ρ photoproduction target is limited by multiple scattering effects on the resolution, the degeneration of the photon beam, and backgrounds. For the calculation of event rates we have chosen 0.2 rad. lengths. Table 2 shows N_T, the number of nuclei/cm^2, for this thickness of various elements.

TABLE 2

Element	A	0.2 X_o	N_T
Beryllium	9	12.6 gm/cm^2	84 $\times 10^{22}$ nuclei/cm^2
Carbon	12	8.5	43
Aluminum	27	4.8	10.7
Copper	63.5	2.56	2.4
Silver	107.9	1.76	0.98
Lead	207.2	1.16	0.34

σ, the total ρ photoproduction cross section

Although each of the three experiments measuring ρ photoproduction up to 5 GeV are internally consistent with the diffraction mechanism, they do not yield the same cross sections. The CEA counter group[1] obtained a differential cross section near 0^o at 4.4 GeV which is two times larger than that obtained by the CEA bubble chamber group.[2] On the other hand, the DESY bubble chamber group[3,8] shows total ρ cross sections which are somewhat smaller than the CEA bubble chamber results.[12] For the lack of anything better, we arbitrarily choose the CEA bubble chamber normalization and divide the counter cross sections by two. Drawing a straight line through the 4.4 GeV counter data for complex nuclei (corrected to $t = 0$ and plotted on log paper as a function of A), and dividing by two gives:

$$\left(\frac{d\sigma}{d\Omega}\right)_{t=0} = 0.9\ A^{1.6}\ \text{mbarn/sterad.}$$

It is more convenient to use:

$$\left(\frac{d\sigma}{dt}\right)_{t=0} = \frac{\pi}{k^2}\left(\frac{d\sigma}{d\Omega}\right)_{t=0}$$

$$= \frac{3.14}{4.4^2} \times 0.9\ A^{1.6} = 0.15\ A^{1.6}\ \text{mbarn/GeV}^2.$$

We then approximate the shape of the differential cross section as :

$$\frac{d\sigma}{dt} = \left(\frac{d\sigma}{dt}\right)_{t=0} e^{-t/q_o^2} ,$$

which gives the total cross section as :

$$\sigma_T = \int_{t_{min}}^{t_{max}} \left(\frac{d\sigma}{dt}\right)_{t=0} e^{-t/q_o^2} \, dt$$

$$\approx q_o^2 \left(\frac{d\sigma}{dt}\right)_{t=0} e^{-t_{min}/q_o^2} ,$$

where q_o can be estimated from proton-nucleus scattering[5] as $q_o = 0.26 \text{ GeV/c} / A^{0.3}$. To a very good approximation the minimum momentum transfer is:

$$t_{min} = \frac{m_\rho^4}{4k^2}$$

and the total cross section formula thus becomes:

$$\sigma_T = \frac{0.067}{A^{0.6}} \; 0.15 \, A^{1.6} \exp\left(- 15 \, A^{0.6} \, \frac{m_\rho^4}{4k^2} \right) \text{ mbarn}$$

$$= 10 \, A \exp\left(- \frac{15}{4} \, \frac{m_\rho^4}{k^2} \, A^{0.6} \right) \mu\text{barn} .$$

Cross sections for several elements are given in Table 3 for $m_\rho = 0.750$ GeV and $k = 5$ and 8 GeV.

TABLE 3

Element	A	$A^{0.6}$	k = 5 GeV exp	k = 5 GeV σ_T	k = 8 GeV exp	k = 8 GeV σ_T
Beryllium	9	3.7	0.84	76 μbarn	0.93	84 μbarn
Carbon	12	4.4	0.81	97	0.92	110
Aluminum	27	7.2	0.70	190	0.87	240
Copper	63.5	12.1	0.60	360	0.82	510
Silver	107.9	16.6	0.45	490	0.73	790
Lead	207.2	24.6	0.31	640	0.63	1300

η, the detection efficiency

Because of the limited solid angle of the detection apparatus we will only be able to detect a small fraction of the ρ's produced. Although a detailed computer calculation will need to be made eventually, we can estimate the detection efficiency by considering it to be the product of three efficiencies, those associated with the ρ production angle θ_ρ, ρ center-of-mass decay angle θ'_{π^-}, and the decay azimuthal angle.

A typical ρ production angle is that corresponding to $q_\perp = q_o$:

$$\theta_\rho = \frac{q_o}{k} .$$

This angle is shown in Table 1 for the various targets; for carbon at 8 GeV it is 0.88^o and about 25% of the ρ's are lost, mainly due to the vertical limits imposed by the magnet pole faces. As the atomic number increases, the ρ production angle distribution shrinks down and the θ_ρ efficiency approaches unity. For counting rate calculations we have taken an average value $\eta_{\theta\rho} = 0.9$.

As is discussed in the preceding section, the focusing properties of the bending magnet are such that for $\pi\pi$ effective mass in the ρ region decays with $|\cos\theta'| \lesssim 0.5$ are accepted. The ρ's are expected to decay with a $\sin^2\theta'$ distribution[4] giving:

$$\eta_{\theta'} \approx 0.7$$

The azimuthal decay angle acceptance is limited by the pole faces at the magnet exit and depends somewhat on θ' and k, a typical value being $\eta_\phi = 6\%$ for k = 8 GeV.

A typical detection efficiency is thus expected to be about:

$$\eta = \eta_{\theta_\rho} \eta_{\theta'} \eta_{\phi} \approx 0.9 \times 0.7 \times 0.06 = 3.8\%$$

N_ρ, expected number of detected ρ's

Combining the factors discussed above yields the counting rates for k = 8 GeV shown in Table 4; at 5 GeV the counting rates are lower by a factor of 2 to 3.

TABLE 4

Number of ρ's detected per hour (180 pulses/sec)

Element	N_ρ(k = 8 GeV)
Beryllium	1300
Carbon	870
Aluminum	480
Copper	220
Silver	140
Lead	80

For the choice made of target thickness as a certain fraction of a radiation length, the counting rates are roughly proportional to $A^{-1}(\sigma \times N_T \propto A \times A^{-2} = A^{-1})$.

IV. RUNNING TIME

We have estimated our running time as follows:

1. Measurement of the ρ coherent cross section at 8 GeV for six elements (e.g., Be^{9}, C^{12}, Al^{27}, $Cu^{63.6}$, Ag^{108}, $Pb^{207.2}$); approximately 2000 ρ's per element . . . . . 60 hrs.
2. Measurement of the ρ coherent cross section at 4 and 6 GeV on carbon and copper, approximately 2000 ρ's each . . . . . 40 hrs.
3. Detailed study of the q^2 distribution including the incoherent region for the light elements (Be, C and Al); approximately 10,000 ρ events for each element (only ~ 5% of which come from incoherent processes). . . . . 45 hrs.
4. Investigation of ϕ, f^o, etc. photoproduction from carbon (8 GeV). . . . . 25 hrs.
5. Beam calibration using our apparatus as an electron pair spectrometer (tungsten stopper removed). . . . . 10 hrs.
6. Background measurements, for example, e^- runs (bremsstrahlung only with no monochromatic photons), target-out runs, random coincidence runs, etc. . . . . 40 hrs.
7. Time lost changing experimental conditions, contingency for equipment failure, etc. . . . . 20 hrs.

Total high intensity running time (180 bursts/sec) . . . . . 240 hrs.

Setup time with low intensity beam . . . . . 50 hrs.

If a larger magnet such as an Atlas or the 54-inch magnet (Perl) can be obtained, the high intensity running time could probably be cut from 240 hours down to about 180 hours.

APPENDIX A

FIRST ORDER OPTICS

Consider the idealized situation shown in Fig. 4; a forward going (0^o) ρ^o meson of mass m_ρ and energy k decays with angle θ' in the center of mass system and $\phi = 0^o$, i.e., in the central plane of the bending magnet. We neglect fringe fields and consider the bending magnet to have constant field B (Weber/m^2 = 10 kG) over a length L (meters). We then have

$$\alpha \approx \frac{L}{R} = \frac{L}{P_\pi/0.3\ B} = \frac{.3\ BL}{P_\pi}$$

where p_π is the lab momentum of the decay pion (GeV/c).

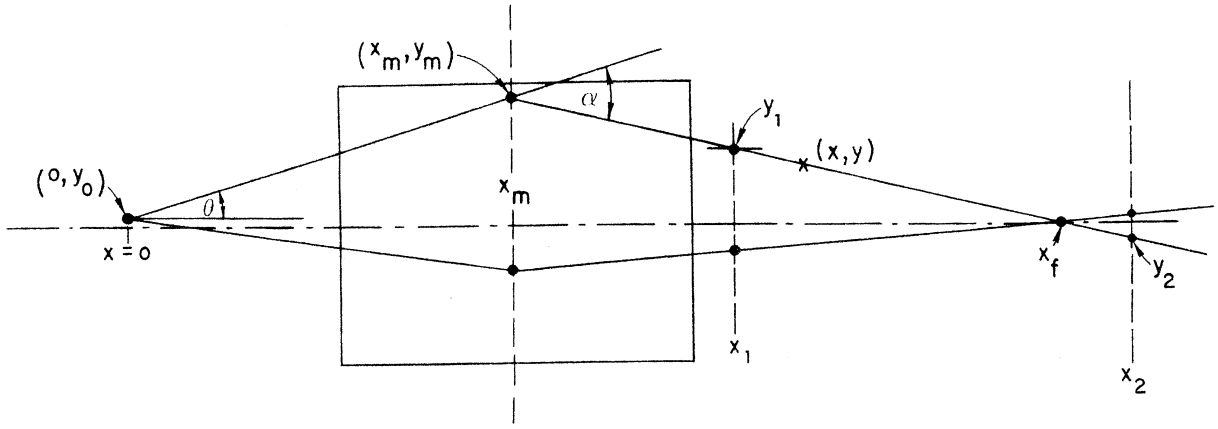

FIG. 4

Using the construction shown in the figure we solve for y in the region after the magnet using the small angle approximation:

$$y = y_m - (\alpha - \theta)(x - x_m)$$

$$= \theta x_m - (\alpha - \theta)(x - x_m)$$

$$= \alpha x_m - (\alpha - \theta)\, x.$$

For a focus we fix the ρ mass and require that y be independent of small variations of θ_{lab} about the symmetry angle (corresponding to 90^o in the center-of-mass):

$$\left(\frac{\partial\alpha}{\partial\theta}\right)_{m_\rho} x_m - \left[\left(\frac{\partial\alpha}{\partial\theta}\right)_{m_\rho} - 1\right] x_f = 0$$

$$x_f = \frac{\left(\frac{\partial\alpha}{\partial\theta}\right)_{m_\rho}}{\left(\frac{\partial\alpha}{\partial\theta}\right)_{m_\rho} - 1} x_m ,$$

where $\partial\alpha/\partial\theta$ is to be evaluated at $\theta' = 90^o$. Note that unlike the usual optical focus, the image distance of the system is directly proportional to the object distance. We evaluate $(\partial\alpha/\partial\theta)_{m_\rho}$ using the expressions

$$\frac{d\alpha}{dp_\pi} = -\frac{\alpha}{p_\pi}$$

$$\left(\frac{\partial p_\pi}{\partial\theta}\right)_{\substack{m_\rho \\ 90^o}} = \left(\frac{p_\pi}{\theta}\right)_{90^o}$$

where the last expression is shown by direct evaluation to be good to better than 1%. We then have

$$\left(\frac{\partial\alpha}{\partial\theta}\right)_{m_\rho} = \frac{d\alpha}{dp_\pi}\left(\frac{\partial p_\pi}{\partial\theta}\right)_{m_\rho}$$

$$= \left(-\frac{\alpha}{p_\pi}\right)_{90^o}\left(-\frac{p_\pi}{\theta}\right)_{90^o}$$

$$= \left(\frac{\alpha}{\theta}\right)_{90^o} .$$

Inserting this value into previous equation gives

$$\boxed{x_f = \left(\frac{\alpha}{\alpha - \theta}\right)_{90^o} x_m} \quad .$$

The y coordinate of the focal point is

$$\begin{aligned} y_f &= \alpha x_m - (\alpha - \theta) x_f \\ &= \alpha x_m - (\alpha - \theta)_{90^o} \left(\frac{\alpha}{\alpha - \theta}\right)_{90^o} x_m \\ &= 0 \end{aligned}$$

i.e., the focus is on the axis.

Rhos of different mass will still focus on the axis, but with a different x_f. Since for $\theta' = 90^\circ$, $p_\pi \approx k/2$, we have $\alpha_{90^o} \propto 1/k$ which is independent of m_ρ. The symmetric pion angle can be approximated as

$$\theta_{90^o} = \eta(k) \frac{m_\rho}{k}$$

where $\eta(k)$ assymptotically approaches unity for $k >> m_\rho$. Differentiating gives

$$\begin{aligned} \frac{dx_f}{dm_\rho} &= \frac{\alpha x_m}{(\alpha - \theta)^2} \left(\frac{d\theta}{dm_\rho}\right)_{90^o} \\ &= \frac{x_f}{(\alpha - \theta)_{90^o}} \frac{\theta_{90^o}}{m_\rho} \end{aligned}$$

$$\boxed{\frac{\Delta x_f}{x_f} = \frac{\Delta m_\rho}{m_\rho} \left(\frac{\theta}{\alpha - \theta}\right)_{90^o}} \quad .$$

In the high energy limit both α and θ go as k^{-1} and x_f is independent of k.

If the ρ's are produced in a very small target at an angle θ_ρ, then the above arguments hold if we simply rotate axes. The focal point instead of being on the x axis is displaced a distance $x_f \theta_\rho$ from which θ_ρ can be obtained. If the ρ production origin is off axis a distance Δy, then the focal point for a $0^o \rho$ is also displaced Δy.

APPENDIX B

RESOLUTION OF THE SYSTEM

An estimate of the experimental resolution of various physical quantities can be obtained using the small-angle first order approximation indicated by Fig. 4. An interaction takes place in the target at position $x=0$, $y=y_o$. A pion comes off at angle θ and is bent through an angle α by the magnet. The horizontal position of the trajectory is measured at x_1 and x_2 which together with y_o (known to within half the target width) gives θ and α as:

$$\theta = \frac{-(x_2 - x_1)y_o + (x_2 - x_m)y_1 - (x_1 - x_m)y_2}{x_m(x_2 - x_1)}$$

$$\alpha = \frac{-(x_2 - x_1)y_o + x_2y_1 - x_1y_2}{x_m(x_2 - x_1)}$$

In actual practice we will measure y at four values of x after the magnet in order to resolve the ambiguity as to which coordinates belong to which pions; this additional information can also be used to reduce the resolution width, but we ignore this possibility here.

If we take*

$$x_m = 1.25 \text{ m}, \quad x_1 = 2.25 \text{ m}, \quad x_2 = 3.5 \text{ m},$$

then the formulas become

$$\theta = -0.8\, y_o + 1.44\, y_1 - 0.64\, y_2$$

$$\alpha = -0.8\, y_o + 2.24\, y_1 - 1.44\, y_2$$

for θ and α in radians and y_i in meters (or mrad - mm).

*These values are somewhat different from those indicated in Section II. In any case, the choice of magnet (and hence the details of geometry) are uncertain at this time and the resolution calculations discussed here are illustrative only. If a magnet field of 20 kG is used instead of the 10 kG discussed here, the momentum resolution will become twice as fine.

In the following we use the usual Gaussian approximation for errors with

$$\sigma_{y_o} = \pm 3 \text{ mm} = 3 \times 10^{-3} \text{ m}$$

$$\sigma_{y_1} = \sigma_{y_2} = \pm 0.5 \text{ mm} = \pm 0.5 \times 10^{-3} \text{ m} .$$

Using these errors we obtain

$$\sigma_\theta = \left\{ (0.8 \times 3)^2 + (1.44 \times 0.5)^2 + (0.64 \times 0.5)^2 \right\}^{\frac{1}{2}} \times 10^{-3}$$

$$= \left\{ 5.8 + 0.5 + 0.1 \right\}^{\frac{1}{2}} \times 10^{-3} = \pm 2.5 \text{ mrad},$$

$$\sigma_\alpha = \left\{ (0.8 \times 3)^2 + (2.24 \times 0.5)^2 + (1.44 \times 0.5)^2 \right\}^{\frac{1}{2}} \times 10^{-3}$$

$$= \left\{ 5.8 + 1.2 + 0.5 \right\}^{\frac{1}{2}} \times 10^{-3} = \pm 2.7 \text{ mrad} .$$

The latter error is related to the momentum resolution

$$\frac{\sigma_p}{p} = \frac{\sigma_\alpha}{\alpha} .$$

For example, a 4 GeV/c particle traversing a 10 kG field 1.83 meters long has a bend $\alpha = 137$ mrad, and the momentum is then measured to $\pm 2.0\%$.

Care must be taken when calculating quantities which are functions of both pions since y_o is the same for both π^+ and π^-. At the symmetry point, $\theta' = 90^o$, many quantities are independent of y_o and the usual simple-minded method of taking $\Sigma \sigma_i^2$ clearly does not work in the case of y_o. Similar difficulties arise when calculating quantities depending on both the angle and momentum of a pion since these quantities are also correlated.

Photon Energy Resolution

For small-momentum-transfer events at high energies

$$k \approx E_\rho \approx p_1 + p_2 = 0.3 \text{ BL} \left(\frac{1}{\alpha_1} + \frac{1}{\alpha_2} \right)$$

$$dk = - 0.3 \text{ BL} \left(\frac{d\alpha_1}{\alpha_1^2} + \frac{d\alpha_2}{\alpha_2^2} \right)$$

Considering for the moment only the uncertainty in y_o, $d\alpha_1 = -d\alpha_2 = \Delta\alpha$,

$$\Delta k = 2 \frac{\Delta\alpha}{\alpha_{90}} \left(p_2 - p_1 \right)$$

where α_{90} is the bend for $p = p_{90^o} = k/2$. For $\theta' = 70^o$, 10 kG, $k = 8$ GeV, etc., this becomes

$$\frac{\sigma_k}{k} = 1.1\,\%$$

from y_o alone. Adding in the effects of σ_{y_1} and σ_{y_2} gives a total uncertainty at $\theta' = 70^o$ of

$$\frac{\sigma_k}{k} = \pm\ 1.5\,\% .$$

Rho Mass Resolution

The effective $\pi_1 \pi_2$ mass is

$$m_\rho^2 = 2\, m_\pi^2 + 2\, E_1 E_2 \left[1 - \beta_1 \beta_2 \cos\left(\theta_1 + \theta_2\right) \right] .$$

Differentiating and using various approximations gives

$$\frac{dm_\rho}{m_\rho} \approx \frac{dp_1}{p_1} + \frac{dp_2}{p_2} + \frac{p_1 p_2}{m_\rho^2} \left(\theta_1 + \theta_2\right)\left(d\theta_1 + d\theta_2\right) .$$

The uncertainty from y_o vanishes at $\theta' = 90^o$; for $k = 8$ GeV, $m_\rho = .750$ GeV, $\theta' = 70^o$ this uncertainty in m_ρ from y_o alone becomes $\pm$ 8 MeV. Taking into account the correlations between p_i and θ_i, the measurements behind the magnet give an additional uncertainty of about $\pm$ 6 MeV. Multiple scattering in the target (0.2 radiation lengths) results in an uncertainty of $\pm$ 7 MeV. Thus we have a total uncertainty of

$$\sigma_{m_\rho} \approx \pm\ 12 \text{ MeV} .$$

Momentum Transfer Distribution Resolution

For small momentum transfer events the 4-momentum transfer to a good approximation is given by the 3-momentum transfer :

$$t \approx q^2 = q_{||}^2 + q_{\perp}^2$$

where we have split the 3-momentum transfer into components parallel and perpendicular to the beam direction. The parallel component is well approximated by

$$q_{||} = \frac{m_\rho^2}{2k} \sim \frac{.56}{2 \times 8} = 35 \text{ MeV/c}$$

and the 3% uncertainty in m_ρ^2 introduces an uncertainty in $q_{||}$ of only 1 MeV/c.

We now split $q_{\perp}^2$ into components in the horizontal (normal to B field) and vertical components, $q_{\perp}^2 = q_H^2 + q_V^2$. The horizontal component is given by

$$q_H \approx p_1\theta_1 - p_2\theta_2$$

which can be differentiated to give

$$dq_H = dp_1\theta_1 - dp_2\theta_2 + p_1 d\theta_1 - p_2 d\theta_2$$

This time the uncertainty from y_o does not vanish at $\theta' = 90^o$; for $m_\rho = .750$ GeV and $k = 8$ GeV this uncertainty is $\pm$ 7 MeV/c at 90^o and does not vary rapidly with θ'. The measurements behind the magnet yield an additional uncertainty of 1 MeV/c (taking into account the $p_i\theta_i$ correlations) so the final uncertainty should be

$$\sigma_{q_H} = \pm 7 \text{ MeV/c} .$$

If the vertical coordinates are measured to $\pm$ 0.5 mm at the positions x_1, and x_2, then

$$\sigma_{q_V} \approx \sqrt{2}\, p_{90^o} \frac{.5 \times 10^{-3}}{3.5 - 2.25}$$

$$= \pm 2.3 \text{ MeV/c}$$

at $k = 8$ GeV. The overall measurement uncertainty in $\vec{q}$ of $\pm$ 7 MeV/c is

slightly smaller than the multiple scattering in the target. The two effects together give a $\pm$ 12 MeV/c uncertainty which is considerably smaller than even $q_o = 50$ MeV/c for lead, and the resolution should not noticeably degrade the coherent q^2 peak.

APPENDIX C

BACKGROUNDS

1. Soft Photons

The principal shower component which escapes the tungsten stopper consists of low energy photons in the region 0.5 to 3 MeV; these photons come off at wide angles and escape through the side of the stopper. Those which are emitted into the solid angle subtended by our detection equipment will contribute to the singles counting rates in the counters and will give spurious sparks in the wire chambers.

The number of photons of energy > 0.25 MeV at a distance $> r$ from the shower axis which cross a plane at depth t has been calculated by Nagel[13] for several values of r (up to $9\ X_o$) and t in lead for a primary electron energy of 1000 MeV. For the number of γ rays escaping from a cylinder of radius R, we have integrated Nagel's numbers over t, $\int N_\gamma\ dt/(\overline{\Lambda \cos\theta})$ where $\overline{\Lambda \cos\theta}$ crudely takes into account the absorption of photons in Nagel's calculation by the lead at $r > R$. For $R = 9\ X_o$ we obtain 15 photons escaping (at all angles) per incident 1 GeV photon. This can be compared with the curves calculated by Völkel[14] (using Nagel's Monte Carlo program) for the energy lost from a cylindrical absorber with radius R and length T (6 GeV photon incident on lead). For $R = 9\ X_o$ she gives a 1.5% energy loss for $T \gtrsim 40\ X_o$. Extrapolating this to 1 GeV gives a 15 MeV energy loss or an average of 1 MeV per photon; this energy corresponds to the peak in the photon spectrum given by Völkel for $t \sim 25\ X_o$. Nagel's tables indicate that for $R = 9\ X_o$, the fraction of γ rays having $\theta < 30^o$ is only 5%; a linear extrapolation to the solid angle subtended by the exit of the 18D72 magnet gives 0.12% (actually should be less since $dN/d\Omega$ falls off in the forward direction). These photons come off predominantly at depths of 20 to $30\ X_o$; very few come from $t > 40\ X_o$ and for our purposes the tungsten stopper is infinitely long. For 10^3 photons of 8 GeV per pulse the number of soft photons escaping from a cylinder of $R = 9$ radiation length is then:

$$N \approx 10^3 \times 8 \times 15 \times 0.0012 = 144/\text{pulse}\ .$$

The absorption length for 1 MeV photons in scintillator plastic is 15 gm/cm^2 and a 1/4 inch counter will absorb $\sim 5\%$ of the photons passing through it. The wire chambers themselves present a very small amount of material for photon

absorption and most of the spurious wire chamber sparks from this background will be caused by recoil electrons from photon absorption in the counters. The number of such sparks is $\lesssim$ 2% of the photon flux (i.e., $\lesssim$ 3 spurious sparks per pulse in each of the wire chambers if N_γ = 144/pulse). Thus, the tungsten absorber will probably need to be somewhat thicker than $\pm 9\ X_o$ especially for the larger solid angle configurations which might be used with other magnets. There is some uncertainty as to the extrapolation of the $R = 9\ X_o$ results. Under the assumption that the electrons have already died out and the additional tungsten absorber is simply attenuating the photons with $\Lambda(k = 1.5\ \text{MeV}) = 3\ X_o = 1$ cm, then for photons at $\theta = 10^o$, each additional centimeter of halfwidth gives a factor of 300 attenuation. This assumption is somewhat optimistic, however, and we hope to obtain Monte Carlo results for our particular geometry; also we plan to get a better feeling for the effect by making runs at Mark III. When discussing the experimental set-up we took 12 cm = $\pm$ 18 radiation lengths as the width of the stopper; this appears to be a very conservative configuration.

2. Stopper Events

The γ ray beam (and its shower) will photoproduce strongly interacting particles in the tungsten stopper as well as in the target. We have calculated the ratio of stopper to target reactions (for stopper and target of the same material) under two different assumptions for the effective number of γ rays as a function of t:

(a) $N_\gamma \propto e^{-\frac{7}{9}t}$, i.e., consider events to come only from primary photons

$$\frac{\text{stopper}}{\text{target}} = \frac{\int_{0.2}^{\infty} e^{-\frac{7}{9}t}\,dt}{\int_{0}^{0.2} e^{-\frac{7}{9}t}\,dt} = \frac{0.856}{0.144} = 6.0$$

(b) N_γ = number of photons with energy > 2 GeV in lead shower initiated by a 6 GeV photon[14]

$$\frac{\text{stopper}}{\text{target}} = 11.5\ .$$

The effective number of photons probably lies somewhere in between, say ~ 8. For runs with low Z targets the ratio of stopper to target events is considerably reduced (roughly as $Z_{target}/Z_{stopper}$).

Consider the 0^o production of ρ^o in the middle of the 12 cm (full width) stopper. For k = 8 GeV and $\theta' = 90^o$, the π's come off at 5^o and must then traverse 6 cm/sin 5^o = 69 cm = 1300 gm/cm^2 of tungsten. Taking the strongly-interacting-particle attenuation length in tungsten as 250 gm/cm^2, the probability of one of the pions (or its shower) escaping is then 0.6%. The probability of their both surviving and possibly looking like an event is only 3×10^{-5}; thus ρ^o's give us no trouble. Events with 3 or 4 fast secondaries may give two or more of these particles through the wire chambers; most of these events will be eliminated by the fitting procedure, however. The vertical height and angle will be measured by the wire chambers behind the magnet. When extrapolated back through the magnet the two trajectories should have the same vertical height (to within errors) at the photoproduction target; the majority (typically 80%) of stopper events will not satisfy this condition. Furthermore, the apparent momentum of the two particles will be required to add up to give (within errors) the monochromatic photon energy. The apparent momentum of a particle coming from the stopper will be larger than its actual momentum by a factor which depends on both the geometry and angle of emission of the particle, but is typically 1.4. For a stopper ρ to appear to have 8 GeV, it must thus be produced by a photon of energy $\sim 8/1.4 = 5.7$ GeV; the number of background photons in the beam[10] within $\pm 8\%$ ($\pm$ three standard deviations) of 5.7 GeV is 9%. A similar rejection rate (or better) should be obtained for more complicated events. The over-all rejection rate is thus expected to be:

Attenuation x vertical constraint x energy constraint

$$\approx \frac{1}{10} \times \frac{1}{5} \times \frac{1}{10} = \frac{1}{500} ,$$

which should be more than ample. Furthermore, the correction for this background can be easily made using the results of a target-out run.

3. Wide Angle Electrons From Target

A fraction of the photons passing through the photoproduction target convert giving an e^+e^- pair:

$$f = 1 - e^{-\frac{7}{9}t} \approx \frac{7}{9}\, t,$$

which for $t = 0.2$ radiation lengths is 15%. Some of the electrons emerge from the target at an angle sufficient to clear the tungsten stopper. Two processes contribute to the angular spread of the electrons: the pair production process itself and subsequent scattering. At small angles both processes are approximated by Gaussians with rms values for the projected angle given by:[15]

$$\text{pair prod.} \quad \theta_y \approx \frac{1.7 \text{ MeV/c}}{p}$$

$$\text{mult. scat.} \quad \theta_y \approx \frac{15 \text{ MeV/c}}{p} \sqrt{\frac{t}{2}} = \frac{4.7 \text{ MeV/c}}{p}$$

where $t/2 = 0.1$ radiation lengths is the average distance over which the electrons multiple scatter. The tungsten stopper is so wide that only electrons which are well out on the tails of the distributions ($\gtrsim$ 20 standard deviations) can pass through the system. In this region the Gaussian approximations are no longer valid and one must examine the wide angle pair production and Moliére scattering formulae.

We have integrated the wide angle scattering formulae of Scott[16] over the acceptance of the apparatus as set up for the small angle ϕ run; this gave approximately 0.015 electrons/burst from the monochromatic part of the photon spectrum and 0.03 electrons/burst from the bremsstrahlung background. For the ρ run geometry, this drops by a factor of ~ 3. A crude calculation of the pair production angular distribution indicates that this process contributes a number of electrons at wide angles which is comparable with that from scattering. These numbers do not depend strongly on the atomic number Z for targets having the same number of radiation lengths.

Wide angle electrons are the dominant component of particles passing through the set of trigger counters. The resultant singles rate affects us in two ways. First, the electrons appear as extraneous tracks in the wire chambers; assuming 0.1 electrons/burst and that no effort is made to reduce the wire chamber memory

time to less than the burst duration of 1.5 to 2 μsec, 10% of the events would have an electron passing through. These events could then be discarded, or we could try fits using first one and then the other of the two tracks having the same sign. Such fitting should eliminate the electron in all but about 2% of the cases (factor of ~ 5 for the vertical constraint and $\sim$ 10 for the energy constraint). Secondly, the wide-angle-electron singles rates dominate the random coincidence background. Taking the singles rate to be 0.1/burst $\approx$ 20/sec, the random coincidence rate is then given by:

$$R = C^2\tau/D = 20^2 \times 10^{-8} \times 3000 = 0.012/\text{sec} = 43/\text{hour},$$

where τ = coincidence resolving time $\approx$ 10 nsec and D = duty cycle = 1/3000. Again assuming a factor of 50 in rejection efficiency, this becomes a background of less than one per hour and thus less than 1% of the ρ counting rate.

4. Neutrons

Neutrons are expected from two sources: the tungsten stopper and the positron beam dump.

A rough rule for giant resonance neutrons is one per 5 GeV incident photon energy or $\sim 10^3$ per pulse from the tungsten stopper. Our detectors subtend only about 2×10^{-3} of 4π solid angle giving about two of these neutrons/pulse through the detectors. Since the wire chambers present very little material in which the neutrons can interact, this background should not be troublesome and in any case is easily identifiable. The flux of neutrons from the positron beam dump is quite uncertain; again the low density of the detectors should avoid any large unhappiness.

APPENDIX D

WIRE CHAMBERS AND ELECTRONICS

We propose to use wire spark chamber modules of the type that have been used for experiments on the Berkeley accelerators. Chambers up to 120×45 cm^2 have been built and there should be no difficulties in constructing chambers required by this experiment, as the construction and performance of this type of chamber is well understood.

Each module consists of four wire planes made of wires stretched on glass epoxy frames. The four planes are arranged to form two independent gaps with two ground planes on the outside and two high voltage planes in the middle which are connected individually to 5000 $\mu\mu$F condensers discharging through the usual spark gap arrangement.

The construction of these chambers is shown in Fig. 5. The plastic frames are 3/8-inch thick and have 0.006-aluminum wires stretched and cemented on them at a density of 24 wires/inch. The module consists of five plastic frames. Two on the outside with 0.002-inch Mylar sheets form the gas tight envelope. The two independent gaps are separated by a blank plastic frame so that the two high voltage planes do not interact and can be read out separately. The two outside planes are the ground planes with wires at right angles to each other. The two high voltage planes have wires strung at right angles to each other but rotated by 45^o relative to the ground planes.

The magnetostrictive wires which sense the spark coordinates are mounted on aluminum rods. The rods are inserted into slots cut into the rims of the plastic frame located between the common bus bar connector and the corresponding wire plane. External connections are made to the first and last wires of each plane to provide start and stop signals for the electronics as well as providing "fiducials" for calibration. The interconnections between the corresponding planes are made through a resistor condenser combination (50 ohms in series with 0.1 μf Mylar capacitors).

Figure 6 shows a photograph of two modules mounted on a stand and spaced by 6 inches relative to each other. The sensitive area of these chambers is 45×55 cm.

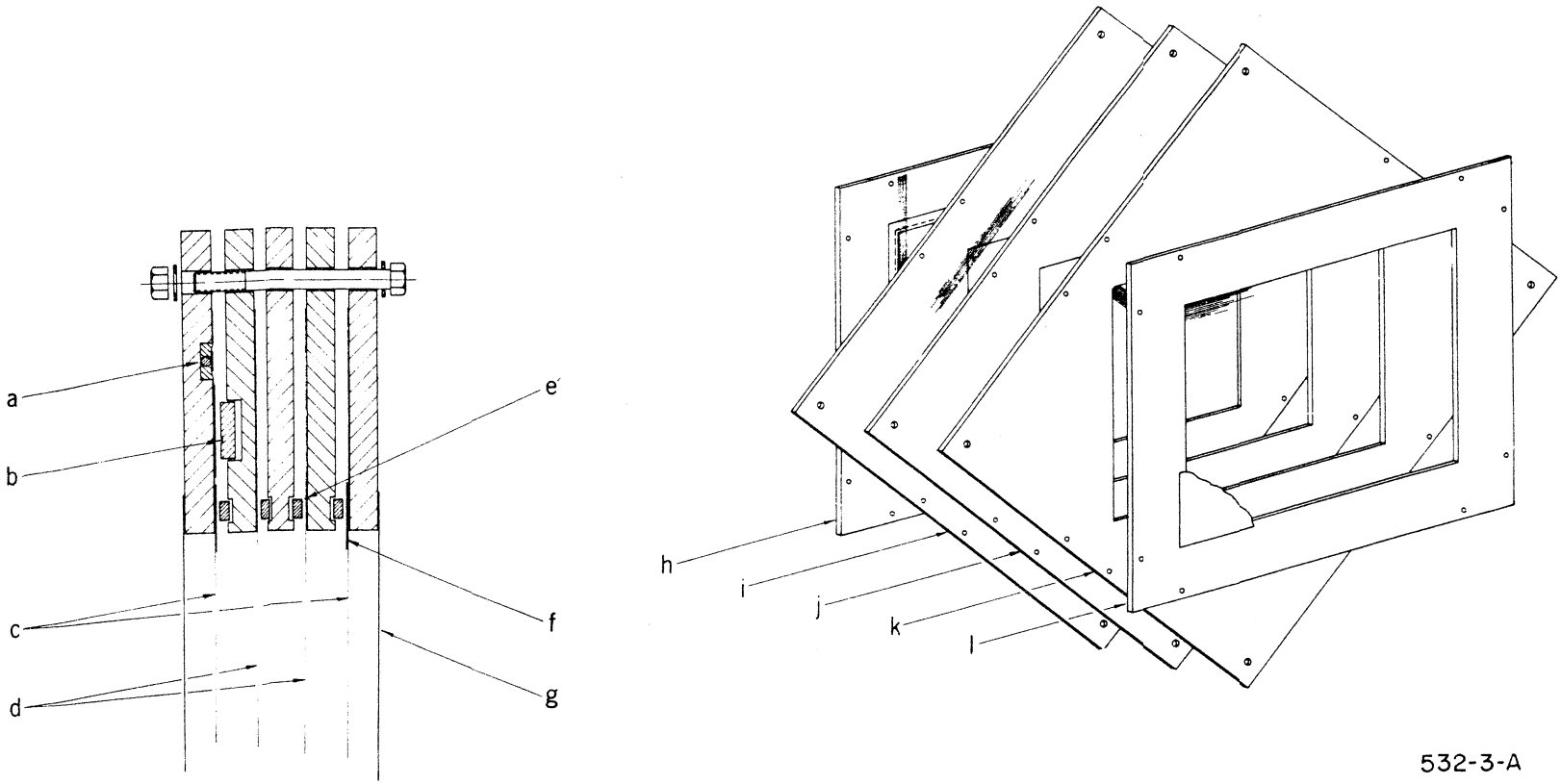

Fig. 5

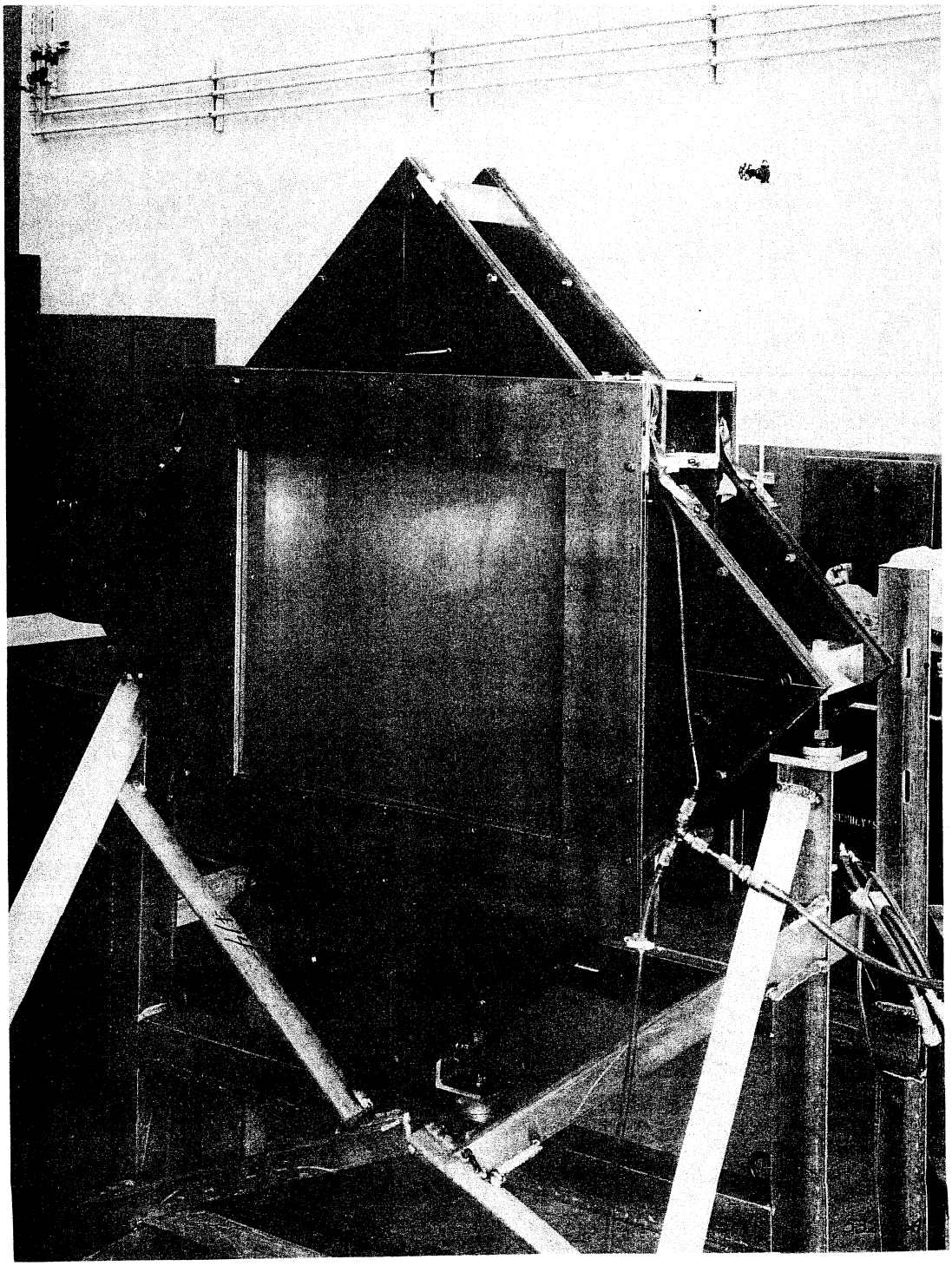

Fig. 6

The magnetostrictive delay lines that we use consist of an iron-cobalt ribbon 0.004×0.020 inch in cross section, held in a groove in an aluminum rod which is inserted in the above mentioned slots in the plastic rims of the chamber. The aluminum is anodized to insulate the ribbon from the holder. At one end the ribbon is mechanically damped by a rubber pad and on the other end it is terminated similarly in a box which holds the receive coil, biassing magnet and signal amplifier.

Figure 7 shows a picture of the magnetostrictive sensor. The pickup coil (E) has 200 turns of No. 50 enameled copper wire threaded on a plastic form, with effective dimensions 0.020 inch long and a diameter of 0.040 inch. The bias magnet is a concentric cylinder of Plastiform magnet (D) which in turn is surrounded by an iron shield (C). The preamplifier consists of a Fairchild 702C integrated circuit mounted on a circuit card (A). With the feedback we use , the effective gain is $\approx$ 150 and provides output pulses up to 1.5 V in amplitude. A diode in the feedback loop serves to clip unwanted polarity signals.

The magnetic shielding of the pickup transducer and the use of iron-cobalt wire ensures that without further precautions the readout will work in the fringing fields of magnets of the order of 1 kG or less.[17]

Four of these wire chambers have been used in a spectrometer arrangement to determine the momenta of pions. With two small chambers on the input side and two larger ones on the output, we found that we could locate particle trajectories to an accuracy of ± 0.3 mm.[18]

We plan to use either the integrated circuit scaler or thin film "core" storage type of readout electronics for digitizing the spark coordinates. The data will be recorded by one of the existing Berkeley data handling systems. One of these systems, called α-63, is a core storage and tape drive system which was built at Berkeley. The other is a system built around a PDP-5 computer having data-break controls and the appropriate interface electronics. Both the α-63 and PDP-5 systems have provisions for monitor displays and continuous checks of performance during the run. Either of these two systems is satisfactory and the choice will be made on the basis of availability at the time. In either case the data output will be stored on tape for processing by the SDS 9300 or the central SLAC computer.

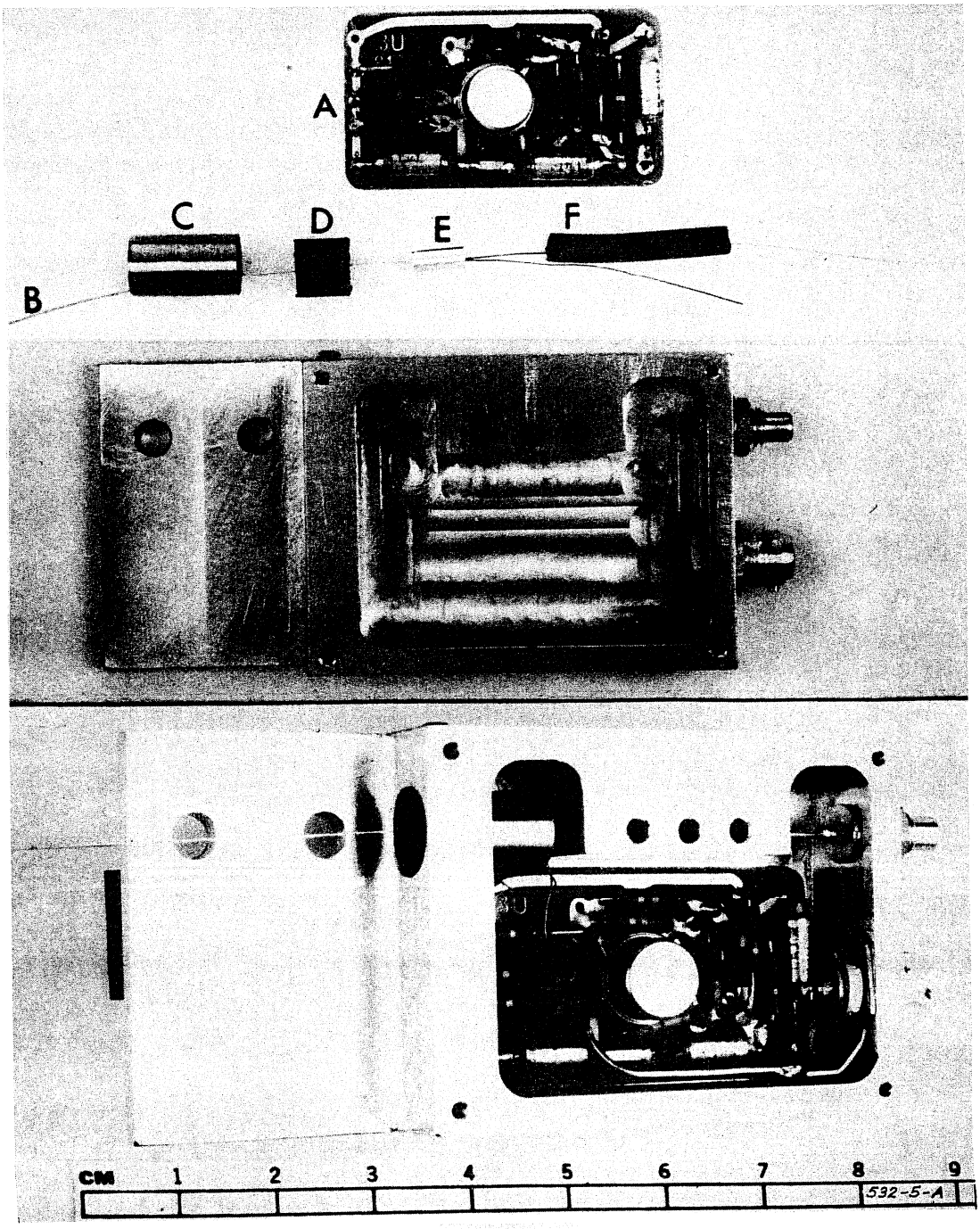

Fig. 7

LIST OF REFERENCES

1. L. J. Lanzerotti et al., Phys. Rev. Letters 15, 210 (1965).
2. H. R. Crouch et al., Phys. Rev. Letters 13, 640 (1964); and to be published in Physical Review.
3. U. Brall et al., Nuovo Cimento 41A, 270 (1966).
4. S. M. Berman and S. D. Drell, Phys. Rev. 133, B791 (1964).
5. G. Bellenttini et al., submitted to Nuclear Phys.
6. S. D. Drell and J. S. Trefil, Phys. Rev. Letters 16, 552 and 832 (1966).
7. J. F. Allard et al., Phys. Letters 19, 431 (1965).
8. W. P. Swanson et al., Bull. Am. Phys. Soc. 11, 358 (1966).
9. Z. Guiragossian, SLAC TN-63-104; J. Ballam et al. SLAC Proposal No. 8.
10. G. Chadwick, SLAC TN-66-13; also reproduced as an appendix of SLAC Proposal No. 8.
11. V. Perez-Mendez and J. M. Pfab, Nucl. Instr. and Methods 33, 141 (1965).
12. Both bubble chamber groups normalize by counting $e^+ e^-$ pairs. Furthermore, they agree on $\sigma_T (\gamma p \rightarrow p \pi^+ \pi^-)$ at the peak of this cross-section near 0.8 GeV.
13. Hans-Hellmut Nagel, Bonn Preprint, January 1965.
14. U. Völkel, DESY 65/6.
15. B. Rossi, High-Energy Particles, published by Prentice-Hall Inc., Englewood Cliffs, N. J., 1952.
16. W. T. Scott, Rev. Mod. Phys. 35, 231 (1963).
17. Kaufman, Perez-Mendez, and Pfab, UCRL-16536 (March 1966).
18. Devlin, Droege, Perez-Mendez and Solomon. Princeton-Penn Accelerator Report PPAD 588E (March 1966).
19. Kirsten, Perez-Mendez and Pfab UCID, August 1965; see also, UCRL-16539 and UCID-2750 (Feb. 1966).